X-ray production by electron excitation, ionization, and capture for F^{q+} ($q = 1$–9) ions in collisions with a He gas target

H. Tawara, Patrick Richard, K. A. Jamison, Tom J. Gray, J. Newcomb, and C. Schmiedekamp
Department of Physics, Kansas State University, Manhattan, Kansas 65506
(Received 4 January 1979)

K x-ray transitions resulting from collisions between F projectiles, with charge states ranging from 1^+ to 9^+, and He atoms have been observed. Production mechanisms leading to projectile *K* x rays include *K*-shell electron excitation, single *K*-shell multiple *L*-shell vacancy production, and electron capture. The measured F *K* x-ray production cross sections range from 10^{-22} cm^2 for low charge states to 10^{-17} cm^2 for incident bare ions. Using calculated average fluorescence yields, the *K*-shell electron excitation, single *K*-shell, single *K*-shell + single *L*-shell, single *K*-shell + double *L*-shell ionization, and electron-capture cross sections have been determined. The measured ionization cross sections are found to decrease with the increase in projectile charge state, whereas single-*K*-shell electron-excitation cross sections increase with the increase in projectile charge state.

I. INTRODUCTION

Recent high-resolution experiments in heavy-ion–atom collisions demonstrate that the satellite structure of x-ray spectra from target atoms depends significantly on the projectile atomic number, its incident energy, and on the physical and chemical states of the target.[1] The x-ray spectra from gas targets are also strongly dependent on the charge state of the projectiles. The satellite structures in *K* x-ray spectra are known to be due to simultaneous multiple ionization and excitation of the inner and outer shells. These multiple processes in turn give rise to different fluorescence yields of the final x-ray emitting atoms. In collisions between heavy ions and heavy target atoms, production mechanisms for the satellite structures are complicated by electron-transfer processes. Similarly, the x-ray satellite structure of projectiles depends on the incident energy, the charge state of the projectile, and on the physical and chemical state of the target.[2,3] For example, Hopkins *et al.*[4] studied the charge state dependence of x-ray spectra of O and F ions in collision with He, Ne, and Ar, and showed that for highly ionized projectiles the electron-capture, electron excitation, and electron exchange processes are responsible for the x-ray production. More recently Fortner and Matthews[5] investigated F*K* x-ray spectra produced in solid and gas targets for 0.5–1.5-MeV/amu F ions and observed a variation of the x-ray spectra between solid and gas targets. They also observed a variation in the relative *K* x-ray intensities with target pressure for gases of Ne and Ar, which was described by collisional quenching of the long-lived innershell vacancy states. Because of the complexity of processes involved in x-ray production in heavy-ion–atom collisions, some qualitative understanding has been obtained from the studies mentioned above, but determination of the projectile *K* vacancy cross sections to specified final states is very limited so far. By specification of the final state the electron excitation, single *K*-shell multiple *L*-shell ionization, and electron-capture processes can be distinguished.

The present investigation is a continuing effort toward a quantitative understanding of heavy-ion–atom collision processes involving the inner-shell electrons as well as the outershell electrons. Helium was chosen as the target in order to minimize the number of collision processes and to facilitate quantitative analysis of the possible processes in *F* K x-ray production. Data for electron excitation, ionization, and electron-capture processes are obtained from the present measurements. The experimental apparatus and procedures are described in Sec. II. In Sec. III the processes responsible for the x-ray production are discussed and quantitative analysis of the measured cross sections based on theories presently available are presented.

II. EXPERIMENTAL PROCEDURE

In the present experiment 15-MeV F^{q+}($q = 2$–9) beams were obtained from the tandem Van de Graaff at Kansas State University. The data for $q = 1$ were obtained with a 5-MeV beam. In addition, a 1.5-MeV proton beam was used to bombard an SF_6 gas target to obtain the F *K* x-ray diagram line. The low charge state F^{q+} beams ($q = 1$–5) were produced directly at the tandem terminal, whereas the high charge state F^{q+} beams ($q = 6$–9) were obtained by using poststripping carbon foils (5 μg/cm^2) placed between the anal-

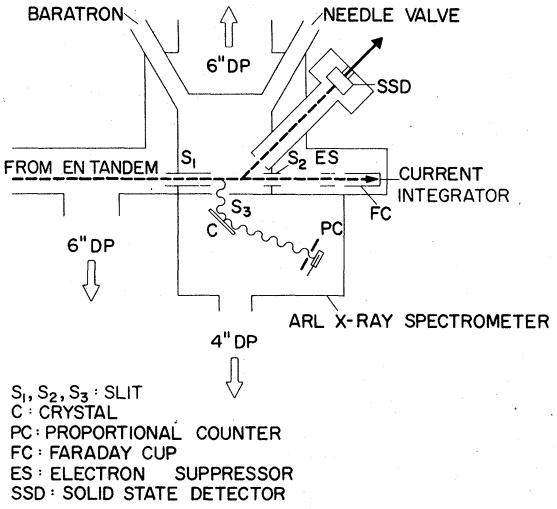

FIG. 1. Schematic of the differentially pumped gas target with the SSD particle monitor, 4-in. ARL curved crystal x-ray spectrometer, and indicated diffusion pumps.

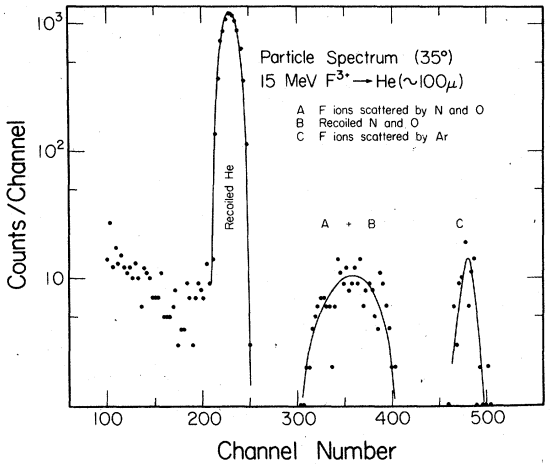

FIG. 2. Particle spectrum obtained for 15-MeV F. The peaks from recoil He and the gas impurities are indicated. The percent of peak *C* in the spectrum is determined by the quality of the window on the proportional counter.

yzing and switching magnets. The F-ion beams entered a collision chamber filled with He gas through an entrance aperture (S_1 = 1.8-mm diam., see Fig. 1) and, after passing through an exit slit (S_2 = 2-mm diam.), were stopped in a Faraday cup. The beam intensity measured at the Faraday cup ranged from 1 μA for lower charge beams to a few nA for F^{9+} beams. The target chamber was attached to an Applied Research Laboratories (ARL) curved crystal x-ray spectrometer, as shown in Fig. 1. The He gas was introduced into the target chamber through a needle valve. Its pressure was monitored with a Baratron gauge and maintained to an accuracy of 5% without using any pressure regulation.

The F *K* x rays produced in collision with the He gas were observed and energy analyzed with the ARL curved crystal spectrometer utilizing a rubidium acid phtalate (RAP) crystal. The x rays entered the spectrometer chamber through an 0.38 × 12.5-mm slit (S_3), which served as an entrance slit for x rays and as a baffle for the He gas. The spectrometer chamber was pumped with a separate 4″ diffusion pump. The x-ray detector was a flow mode proportional counter with a 2μ-Mylar window operated at atmospheric pressure using a 90% argon-10% methane (P10) gas.

Small amounts of heavy impurity gases give rise to large fluorine x-ray production compared to He gas. The target constituents were monitored by a solid-state detector (SSD) placed inside the target gas chamber at 35° with respect to the incident beam direction. This detector recorded the scattered projectiles and recoils from the gas cell. Recoil He ions were clearly separated from the recoil residual N and O, and scattered F from N and O and from Ar which diffused through the proportional counter window. A sample particle spectrum is given in Fig. 2. Spectra taken with a different window on the proportional counter contained no trace of Ar over a similar counting period. The data were accumulated only when the impurity peak counts amounted to less than 1% of

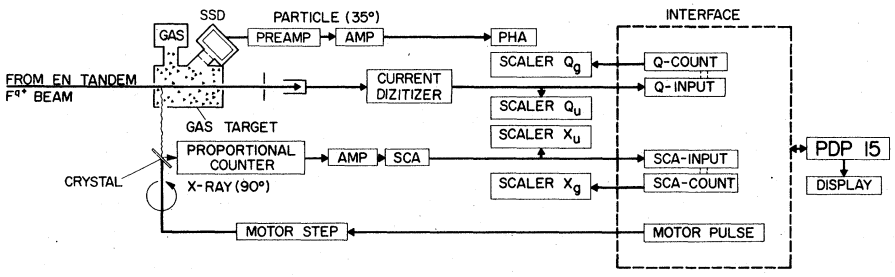

FIG. 3. Schematic of the electronics for the x-ray counting, particle counting, and beam integration. A gated (*g*) and ungated (*u*) scalers recorded both x-ray counts and charge integration counts to account for the dead time incurred during motor stepping of the spectrometer. The particle PHA was turned on-off by the PDP-15 directly.

total particle counts.

X-ray spectra were taken through an electronic controller connected to a PDP-15 computer as described previously.[2] The control circuit is shown in Fig. 3. A dead-time correction factor Q_g/Q_u $(=X_g/X_u)$ was used to obtain the corrected number of He-recoil ions since the interface has no external dead-time gate to control the particle pulse height analyzer (PHA). The PHA was, however, turned on-off by the PDP-15 in sequence with the interface. The x-ray counts in a particular peak were normalized to the number of recoil helium atoms after correcting the x-ray intensity for transmission through the proportional counter window and for reflectivity from the crystal. The transmission correction factors depend on the x-ray energies and ranges from 9.10 for the lowest energy to 1.87 for the highest energy.[6] The reflectivity is only slightly dependent on the x-ray energy.[7] Furthermore, the correction was made for the partial decay in flight[4] of the metastable two electron $(1s2p)^3P$ state ($\tau \simeq 0.5$ nsec) of F ions.[8] This correction factor is 1.13 at 15 MeV for the slit geometry used in this experiment.

III. RESULTS AND DISCUSSION

A. X-ray spectra

The F K x-ray spectra were taken by scanning the energy ranges 660–760 eV and 800–1130 eV separately with the incident F projectile charge states of interest. The low-energy x-ray region is shown in Fig. 4 for 15-MeV F^{2+}, F^{3+}, F^{4+}, and F^{5+}, for 5-MeV F^{+1}, and for 1.5-MeV H^+ on SF_6. The low-energy x-ray region is also shown in Fig. 5 for F^{6+}, F^{7+}, F^{8+}, and F^{9+} beams. The x-ray transitions in the low-energy region (Figs. 4 and 5) are labeled according to the electron configuration KL^n of the initial state of the transition. The simple two-electron K x-ray energy spectrum of the KL configuration can be clearly seen in the F^{8+} spectrum in Fig. 5. The two peaks are for the decay of the He-like $1s2p(^1P)$ (highest energy) and $1s2p(^3P)$ (lowest energy) initial states formed by electron capture.[9] The largest peak for incident F^{6+} is the Li-like $KL^2(^2P)$ transition formed by excitation. The lowest-energy x-ray observed for incident F^{7+} and F^{6+} is the Li-like $KL^2(^4P)$ state. In Fig. 4 the remaining peaks are identified as the KL^7 (diagram line) through KL^3 (Be-like) transition. For the beams given in this figure (F^{2+}–F^{5+}) the amount of Li-like $KL^2(^4P)$ contained in the KL^3 peak is neglected. In the high-energy x-ray region (Fig. 6) the H-like and He-like transitions are labeled by the electron configurations np and $1snp$ (beginning with the $1s3p$ configuration), respectively. Table I contains a list of the transition labels discussed above, the presently observed transition energies, previously measured transition energies,[10] calculated transition energies[11,12] and the assigned transitions. The x-ray energy calibration is based on the $1s2p(^1P) - 1s^2(^1S)$ and $2p - 1s$ transitions.[10] The observed and calculated energies are in good agreement. The two unlabled transitions at

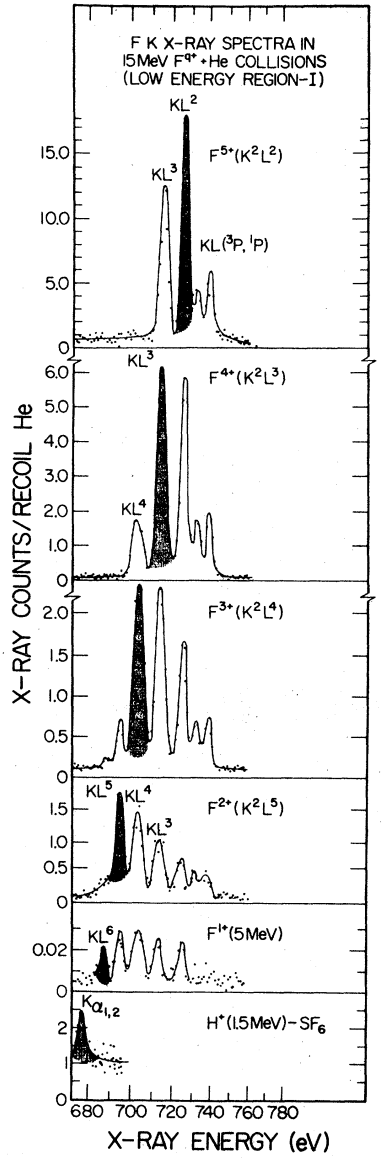

FIG. 4. F K x-ray spectra in the low-energy region 660–760 eV as obtained with incident 1^+–5^+ F on He and H^+ on SF_6. This energy region contains the KL^n–K^2L^{n-1} transitions labeled by the initial state of the transition. The electron configuration of the incident projectiles are also given. The shaded peak is for transitions resulting from single K-shell ionization.

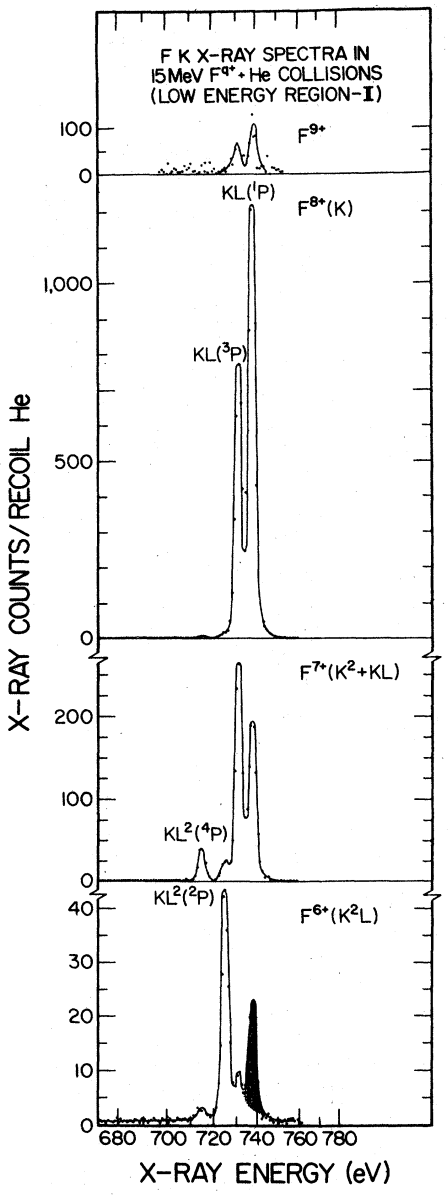

FIG. 5. F K x-ray spectra in the low-energy region for incident F^{6+}–F^{9+} beams (see caption 4).

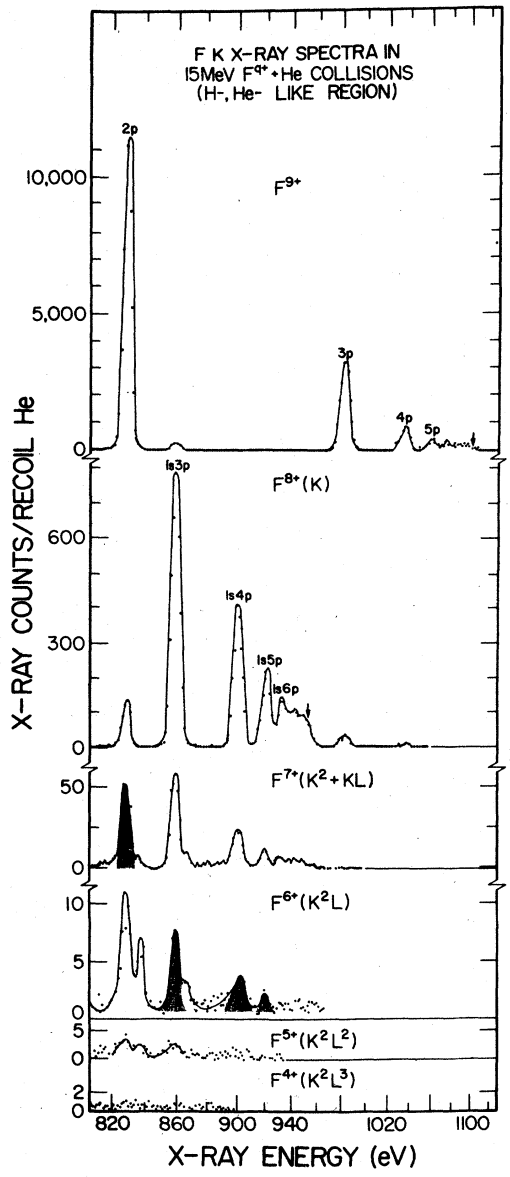

FIG. 6. F K x-ray spectra in the high-energy region 800–1130 eV as obtained with incident F^{4+}–F^{9+} beams. The energy region contains the np-$1s$ (hydrogenic series) and the $1snp(n \geq 3)-1s^2$ (He-like series).

836.7 and 866.2 eV observed in the incident F^{6+} induced spectrum are assigned to excitation of Li-like configurations and have not been previously reported.

B. Pressure dependence

The K x-ray yields for each transition were measured as a function of the target gas pressure. The x-ray yields for the KL^5, KL^4, KL^3, and KL^2 transitions and for the recoil He ions are given in Fig. 7 for incident F^{9+} and are linear with gas pressure over the range of 20–120 mTorr. The pressure dependence for the $1s2p(^1P)$ and $1s2p(^3P)$ transitions for incident F^{8+} projectiles are also linear with pressure as shown in Fig. 8. The fluorine $^3P/^1P$ intensity ratios change with gas pressure for Ne and Ar targets due to collisional quenching of the metastable ^3P states in the target gas.[5] However, for a He target the $^3P/^1P$ ratios are constant in the 20–120 mTorr pressure range as shown in Fig. 8 for a F^{8+} beam. The calculated quenching cross section[13] for the ^3P state of F ions in He is a factor of 20 smaller than that in Ne.

TABLE I. Transition energies in units of eV of F K x rays in F + He collisions.

Transition labels[a]	Experimental energies Present	Kauffman[b]	Calculated energies House[c]	Tunnell[d]	Transition
KL^8	677.0	...	...	677.8	$1s2s^m2p^l \rightarrow 1s^22s^m2p^{l-1}$ $(m+l=8)$
KL^7	...	...	680.4	681.7	$1s2s^m2p^l \rightarrow 1s^22s^m2p^{l-1}$ $(m+l=7)$
KL^6	686.5	...	685.4	687.4	$1s2s^m2p^l \rightarrow 1s^22s^m2p^{l-1}$ $(m+l=6)$
KL^5	694.1	...	692.2	694.6	$1s2s^m2p^l \rightarrow 1s^22s^m2p^{l-1}$ $(m+l=5)$
KL^4	702.3	...	700.5	702.4	$1s2s^m2p^l \rightarrow 1s^22s^m2p^{l-1}$ $(m+l=4)$
KL^3	713.0	...	710.4	711.1	$1s2s^m2p^l \rightarrow 1s^22s^m2p^{l-1}$ $(m+l=3)$
KL^2	714.8	715.1	...	714.7	$1s2s2p(^4P) \rightarrow 1s^22s$
KL^2	725.3	724.8	724.2	725.0	$1s2s2p(^2P) \rightarrow 1s^22s$
$KL(^3P)$	731.0	731.1	...	730.7	$1s2p(^3P) \rightarrow 1s^2$
$KL(^1P)$	737.7	737.7	736.0	735.6	$1s2p(^1P) \rightarrow 1s^2$
$2p$	827.4	827.4	...	827.5	$2p \rightarrow 1s$
	836.7	...	...	836.5[e]	$1s2s3p[^2P] \rightarrow 1s^22s[^2S]$
$1s3p$	858.3	857.5	...	...	$1s3p \rightarrow 1s^2$
	866.2	...	...	863.5[f]	$1s2s4p[^2P] \rightarrow 1s^22s$
$1s4p$	900.1	899.7	...	...	$1s4p \rightarrow 1s^2$
$1s5p$	919.1	919.6	...	...	$1s5p \rightarrow 1s^2$
$1s6p$	932.1	930.3	...	...	$1s6p \rightarrow 1s^2$
$1s7p$	939.8	...	...	...	$1s7p \rightarrow 1s^2$
↓	956.5	954.5	...	...	series limit (He)
$3p$	982.3	981.0	...	980.7	$3p \rightarrow 1s$
$4p$	1034.5	1034.9	...	1034.3	$4p \rightarrow 1s$
$5p$	1060.8	1059.0	...	...	$5p \rightarrow 1s$
$6p$	1072.9	...	...	...	$6p \rightarrow 1s$
$7p$	1080.1	...	...	...	$7p \rightarrow 1s$
↓	1104.4	1103.5	...	...	series limit (H)

[a] These labels are used in identifying the peaks in Figs. 4, 5, 6, and 9.
[b] Taken from Ref. 10.
[c] Taken from Ref. 11.
[d] Taken from Ref. 12.
[e] There are two ^2P transitions, one at 836.5 eV and one at 829.2 eV. The 836.5-eV transition has a larger fluorescence yield.
[f] There are two ^2P transitions, one at 863.5 eV and one at 871.7 eV. The 863.5-eV transition has a larger fluorescence yield.

C. Correspondence between production mechanisms and observed transitions as a function of incident charge state

The measurement of the projectile x-ray production cross sections in high resolution allows one to assign uniquely various production mechanisms to the observed x-ray transitions. The assignment of a transition to a particular production mechanism depends on the incident charge state of the projectile. Examples of the assignments are given in Fig. 9.

1. No initial K vacancies

Figure 9(a) presents an example of a projectile with no initial K vacancies (F^{4+}).

a. K-shell electron excitation. The lowest-energy transition ($KL^4 \rightarrow K^2L^3$) is from an initial state with the same number of electrons as the incident projectile and hence the production mechanism leading to this transition is excitation of a single electron from the K shell to the L shell. Excitation from the K shell to the M shell will result in $2p \rightarrow 1s$ and $3p \rightarrow 1s$ K x-ray transitions as illustrated in Table II. For incident $F^{4+}(K^2L^3)$ this excitation is to the KL^3M configuration with decay to either the K^2L^2M or K^2L^3 final configuration with calculated transition energies[12] of 709.3 and 779.5 eV, respectively. No evidence for the higher-energy transition is observed and the lower-energy transition which is more probable falls between the $KL^4 \rightarrow K^2L^3$ and $KL^3 \rightarrow K^2L^2$ but closer to the latter transition (713.0 eV).

b. K-shell ionization. The next-highest-energy transition ($KL^3 \rightarrow K^2L^2$), which is cross hatched in the figure, is from an initial state with one less electron than the projectile and hence the production mechanism leading to this transition is ionization of a single K-shell electron. The transitions assigned to single K-vacancy production (ionization) for each incident projectile charge state are the cross-hatched peaks in Figs. 4–6 as in the example in Fig. 9(a).

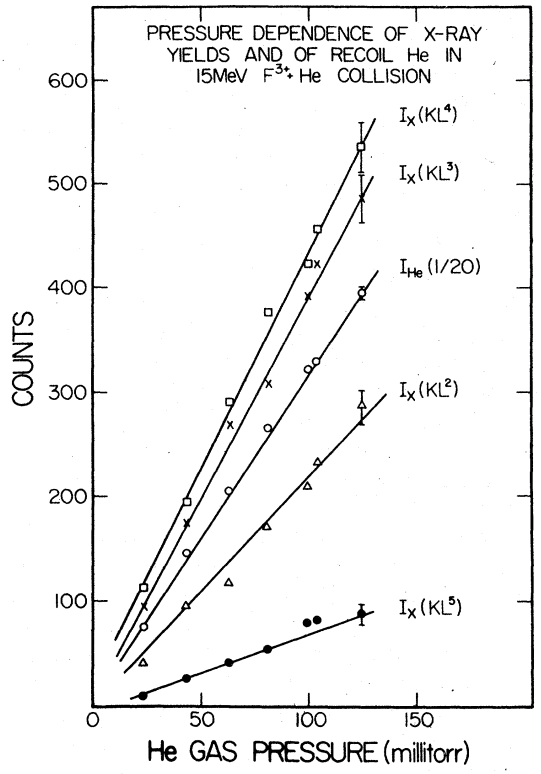

FIG. 7. Pressure dependences of the x-ray yields of each of the peaks KL^2–KL^5 in the 15-MeV F^{3+}+He spectra are linear with gas pressure in the range of 20–120 mTorr. The curve labeled I_{He} is the yield of the recoil He ions.

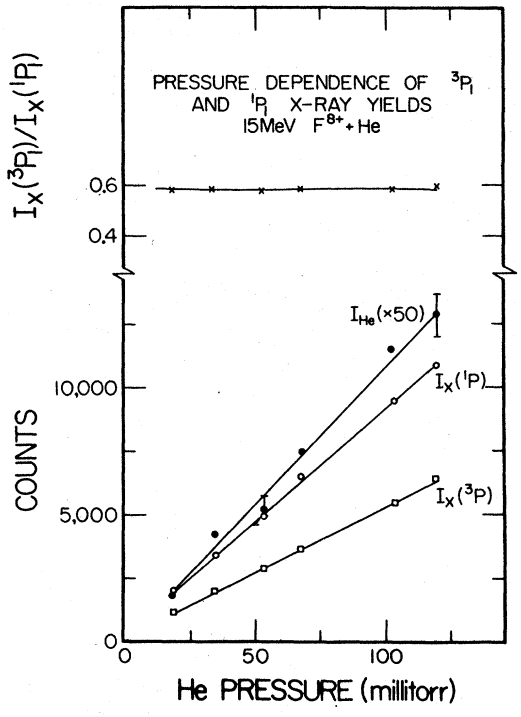

FIG. 8. Pressure dependences of the $1s2p(^1P_1)$, $1s2p$ $(^3P_1)$, and recoil He yields from 15-MeV F^{8+}+He collisions. The ratio of the $^3P_1$ to the $^1P_1$ yields is given in the upper part of the figure. This ratio of yields is constant over the pressure range studied.

The higher-energy peaks (KL^2 and $KL(^3P, ^1P)$ are due to single K-multiple L-shell ionization.

2. Initial K vacancies

Figure 9(b) presents an example for a projectile with an initial K-shell vacancy (F^{8+}).

a. K-shell electron excitation. The peaks labeled np are the H-like transitions and hence assigned to excitation of a single projectile electron from the K shell to the higher shells.

b. Electron capture. The He-like series labeled as $1snp$ results from capture of an electron into the np and higher orbits of the projectile. For projectiles with no initial K-shell vacancies (F^{q+}, $q \leq 6$) the single capture process does not result in a K x-ray. The incident F^{7+} ion beam contains metastable $1s2s(^3S)$ ions which contain K-shell vacancies and must be considered as a special case.

3. Production mechanisms

In the following subsections, a brief description of the production mechanism for each peak for the incident projectile $F^{q+}(K^nL^m)$ is given.

a. $F^{2+}(K^2L^5)$. The four lowest-energy peaks in Fig. 4 (F^{2+}) are easily assigned in the order of increasing energy to 1 K-shell electron excitation (KL^6) (small shoulder at 686.5 eV), 1 K-shell electron ionization (KL^5), 1 K-shell +1 L-shell electron ionization (KL^4), and 1 K-shell +2 L-shell electron ionization (KL^3). Peaks corresponding to higher ionization states for this projectile are not included in the present analysis.

b. $F^{3+}(K^2L^4)$. The first four peaks beginning at an x-ray energy of 694.1 eV in Fig. 4 (F^{3+})KL^5, KL^4, KL^3, and KL^2 are assigned to the 1 K-shell excitation, 1 K-shell ionization, 1 K-shell + 1 L-shell ionization, and 1 K-shell + 2 L-shell ionization mechanisms, respectively. As in the case of F^{2+} the higher-energy peaks are not included in the analysis.

c. $F^{4+}(K^2L^3)$. The assignments of production mechanisms for this incident beam are discussed above in the example using Fig. 9(a).

d. $F^{5+}(K^2L^2)$. The first peak KL^3 at 713.0 eV in Fig. 4 is due to 1 K-shell excitation. One K-shell excitation is becoming significant because the number of available vacancies in the $2p$ shell is getting large. The second peak is due to 1 K-shell ionization. The third and fourth peaks correspond to the ^3P and ^1P transition of $(1s2p)$He-

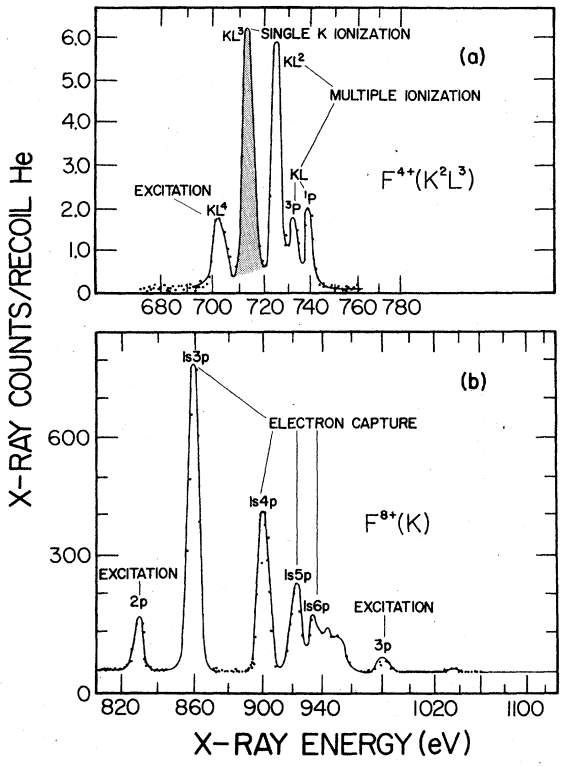

FIG. 9. (a) K x-ray spectrum from 15-MeV $F^{4+}(K^2L^3)$ + He with the designation of the processes leading to each of the peaks. This represents a case with no K-shell vacancies in the incident projectile. (b) K x-ray spectrum from 15-MeV $F^{8+}(K)$ + He with the designation of the processes leading to each of the peaks. This represents a case with a K-shell vacancy in the incident projectile.

like F ions and are due to 1 K-shell + 1 L-shell ionization. Note that the $KL(^3P)$ peak is decreased in intensity compared to the $KL(^1P)$ peak. For this projectile charge state, some low-intensity peaks are observed in the high-energy region (see Fig. 6). Note that even though the incident projectile ($K^2L^2 = 1s^22s^2$) has no $2p$ electrons, the $1s2s2p$ configuration is present following the collision as evidenced by the observation of the $1s2s2p(^2P) \rightarrow 1s^22s(^2S)$ x ray. This indicates that the $2s$ and $2p$ levels get substantially mixed during the collision. It is also known that the $1s2s2p(^4P)$ state (714.8 eV) lies at an energy similar to the $1s2s^22p$ configuration energy (713 eV). We have not corrected the 1 K-shell excitation or the 1 K-shell ionization intensities for this effect since there is no way to obtain the ^4P fraction from our experiment.

TABLE II. Calculated[a] average $2p \rightarrow 1s$ and $3p \rightarrow 1s$ transition energies from $1s2s^22p^N3p$ configurations of F^{+q} for $N = 1, 2, 3, 4$.

Initial configuration	Transition energies (eV) $2p \rightarrow 1s$	$3p \rightarrow 1s$
$1s2s^22p3p$ (KL^3M)	709.3	779.5
$1s2s^22p^23p$ (KL^4M)	699.8	754.6
$1s2s^22p^33p$ (KL^5M)	692.0	732.3
$1s2s^22p^43p$ (KL^6M)	685.7	712.6

[a]Calculations by Tunnell and Bhalla, Ref. 12.

e. $F^{6+}(K^2L)$. The second peak $KL^2(^2P)$ at 725.3 eV corresponds to 1 K-shell excitation to the $1s2s2p(^2P)$ state and is very intense (Fig. 5). The first peak $KL^2(^4P)$ at 714.8-eV cannot be formed from the ^2S ground state by Coulomb excitation. The small ^4P intensity may be due to electron exchange.[14] H-like and additional He-like and Li-like peaks are seen in the high-energy region of the x-ray spectrum (see Fig. 6). The He-like transitions result from 1 K-shell ionization. Note once again that even though no $2p$ electrons are present in the incident projectile, there are substantial amounts of the $1snp$ and np configurations after the collision. The H-like transitions result from 2 K-shell ionization or possibly 1 K-shell + 1 L-shell ionization + 1 K-shell excitation. It is interesting to note that two peaks, one just above the $2p$-$1s$ transition and one above the $1s3p$-$1s^2$ transition, are significant. Hartree-Fock calculations show that these peaks may be due to Li-like transitions $1s2s3p \rightarrow 1s^22s$ and $1s2s4p \rightarrow 1s^22s$, respectively (see Table I). These peaks are due to the $1s \rightarrow 3p$ and $1s \rightarrow 4p$ excitation channel.

f. $F^{7+}(K^2+KL)$. The spectrum in the low-energy region of the x-ray spectrum (see Fig. 5) produced by the F^{7+} beam has the interesting features that the $1s2s2p(^4P) \rightarrow 1s^22s(^2S)$ transition labeled $KL^2(^4P)$ is larger than the $1s2s2p(^2P) \rightarrow 1s^22s(^2S)$ transition labeled $KL^2(^2P)$ and that the $1s2p(^3P) \rightarrow 1s^2(^1S)$ transition labeled $KL(^3P)$ is larger than the $1s2p(^1P) \rightarrow 1s^2(^1S)$ transition labeled $KL(^1P)$. Both of these effects are attributed to the presence of the metastable $1s2s(^3S)$ state in the projectile beam. This metastable fraction is established in the post-stripper foil used to obtain the 7+ beam. The $1s2p(^3P)$ state is formed by the excitation of the $1s2s(^3S)$ component of the beam, giving rise to a larger $^3P/^1P$ ratio (see discussion below). The $1s2s2p(^4P)$ state is formed by capture directly into the $1s2s(^3S)$ metastable component, giving rise to a large ^4P contribution. The spectrum in the high-energy region (see Fig. 6) is given for completeness, but due to the complicated nature of the excitation process, the cross sections are not included in our systematics given in Sec. III G.

g. $F^{8+}(K)$. Two different kinds of x-ray emission peaks are observed: H-like and He-like peaks

(see Figs. 5 and 6). The H-like peaks ($2p$-, $3p$-, $4p$-$1s$) are clearly seen and are due to single K-shell electron excitation. The He-like peaks ($1s2p\,^3P$, ^1P-, $1s3p$-, $1s4p$-, $1s5p$-, $1s6p$-, $1s7p$-, $1s8p$-$1s^2$) are observed and are due to the one-electron capture. As shown in a separate paper,[15] the electron-capture cross section (σ_{ec}) is strongly dependent on the projectile energy, whereas the electron excitation cross section (σ_{ee}) is almost constant from 10 to 40 MeV. At 10 MeV, σ_{ec} is three orders of magnitude larger than σ_{ee} but at 40 MeV σ_{ee} becomes one order of magnitude larger than σ_{ec}.

h. F^{9+} (bare nucleus). Spectra from F^{9+} ions are very simple because all transitions are due to the electron capture. The $2p$-, $3p$-, $4p$-, $5p$-, $6p$-, $7p$-$1s$ peaks and series limit are easily observed. Low-intensity peaks due to double electron capture to He-like ions are observed. The ratio of double to single capture is approximately 0.01.

D. X-ray production cross sections

A summary of the x-ray production cross sections obtained from the K x-ray spectra as discussed in the above section for incident F^{2+} to F^{9+} (except F^{7+}) projectiles are given in Fig. 10. The cross sections are obtained by normalizing the x-ray counts per recoil He ion to the measured total x-ray production cross sections of Guffey[16] for F^{8+} + He at 15 MeV. The lines labeled $q+$ connect points obtained for the same incident charge state. One K-shell excitation, 1 K-shell ionization, 1 K-shell + 1 L-shell ionization cross sections for incident projectile F^{q+} ($q^+ = 2^+ - 6^+$) are plotted versus q at q, $q+1$, and $q+2$, respectively, on the abscissa. For example, the $1s \rightarrow 2p$ electron excitation and the 1 K-shell ionization cross sections for $q = 4$ are the points plotted at 4 and 5 on the abscissa. K-shell excitation and single nl electron-capture cross sections for incident F^{q+} ($q^+ = 8^+$ and 9^+) are plotted at q and $q-1$, respectively. It is seen that the x-ray production cross sections span more than four orders of magnitude.

E. Charge-state dependence of $^3P/^1P$ ratios

Recently Fortner and Matthews[5] reported the variation of the $^3P/^1P$ ratios of F^{q+} ions with q for targets of Ne, Ar, and Kr. Additional data on the $^3P/^1P$ ratios are shown in Fig. 11 as a function of the charge state (q) of F^{q+} ions incident on a He target. With increasing charge state, this ratio decreases smoothly from a value somewhat greater than unity for low-charge states to about 0.5 for F^{6+} and again increases

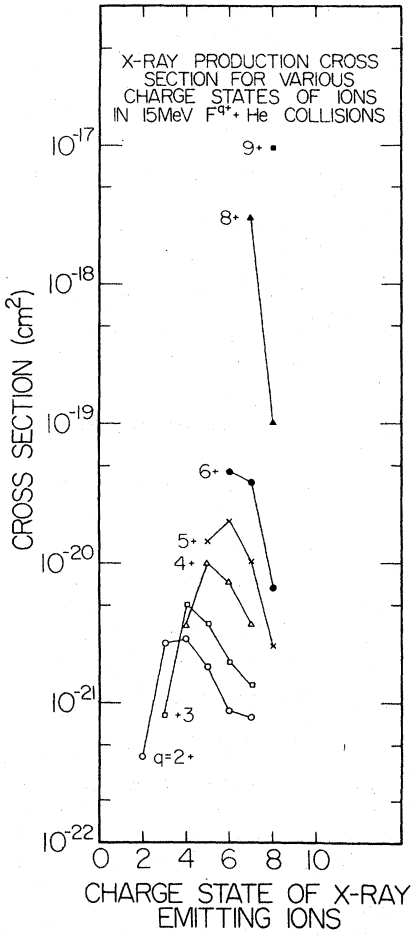

FIG. 10. X-ray production cross sections for 15-MeV F^{q+} + He ($q = 2$–6, 8, and 9) in units of cm^2. See discussion in text for explanation of labels.

to 0.7 for F^{9+} ions. The exceptionally high value of the $^3P/^1P$ ratio for F^{7+} ions is due to the existence of the $1s2s(^3S)$ metastable component in the incident F^{7+} beam. For the F^{7+} ground state, the $^3P/^1P$ ratio should be small since excitation to the ^3P state from the ground state requires spin-flip, which is prohibited under dipole excitation.

For lower-charge-state ions which have many electrons, it is expected that the excited states formed by multiple electron processes are statistically populated, i.e., the $^3P_1/^1P_1$ ratio would be unity. This is nearly the case for low-charge-state ions. For higher-charge-state ions, the nonspin flip electron excitation selection rule becomes more strict. If it were possible to obtain a pure $1s^2$ F^{7+} beam, it is predicted that the charge-state dependence of the $^3P/^1P$ ratio would exhibit a cusplike behavior with a minimum at $q = 7$.

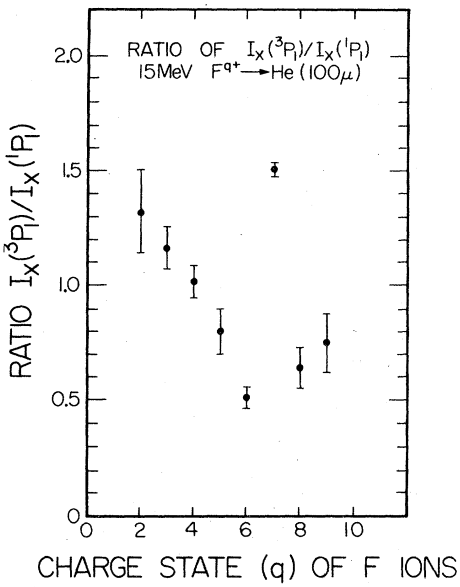

FIG. 11. Ratio of intensities of the $1s2p(^3P)$ decay to the $1s2p(^1P)$ decay of F is displayed as a function of the incident projectile charge state for 15-MeV F^{q+}+He. For $q=7$ the process is electron excitation of the beam, for $q>7$ the process is electron capture, and for $q<7$ the process is ionization. The exceptionally high ratio at $q=7$ is due to the preferential excitation of the $1s2p$ (^3P) state from the metastable $1s2s(^3S)$ component in the incident beam.

F. Average fluorescence yields of various ionization states

To convert the measured x-ray production cross sections into the ionization cross sections, the fluorescence yields must be known. No experimental or theoretical average values of the fluorescence yields of F^{q+} ions with various ionization states have been reported previously, except for F^+. The fluorescence yields for all the possible electron configurations $(1s2s^m2p^l)$ were calculated by Tunnell and Bhalla[17] based on the method developed by Bhalla[18] using the nonrelativistic Hartree-Fock-Slater atomic model. By weighting the possible electron configurations assuming a statistical population distribution of states, the average fluorescence yields are obtained, as given in Table III. The calculated average fluorescence yields increase sharply for F^{q+} $(q \geq 5)$ ions. Also shown are the average fluorescence yields obtained based on the statistical scaling model of Larkins.[9] For $q \leq 4$, the agreement between the two methods is fairly good. The two methods of calculating the fluorescence yield disagree for $q \geq 5$, as discussed by Bhalla *et al.*[19]

G. Single, double, and triple ionization cross sections for various charge states

The measured x-ray production cross sections for single K, single K + single L, and single K +double L-shell ionization are converted to ionization cross sections using the fluorescence yields from Ref. 17. These results are shown in Fig. 12.

The ionization cross sections decrease with increases in the charge state of the projectiles.

TABLE III. Average fluorescence yields for various charge states of F^{q+} ions (×100).

q	Configuration	ω_q	Weight	$\tilde{\omega}$	$\tilde{\omega}$ [a]
0	$1s^12s^22p^6$	1.13	2	1.13	1.13
1^+	$1s^12s^22p^5$	1.17	12		
	$1s^12s^12p^6$	1.41	4	1.23	1.31
2^+	$1s^12s^22p^4$	1.27	30		
	$1s^12s^12p^5$	1.57	24		
	$1s^12p^6$	1.30	2	1.40	1.48
3^+	$1s^12s^22p^3$	1.56	40		
	$1s^12s^12p^4$	1.86	60		
	$1s^12p^5$	1.75	12	1.74	1.85
4^+	$1s^12s^22p^2$	1.83	30		
	$1s^12s^12p^3$	3.16	80		
	$1s^12p^4$	2.24	30	2.68	2.23
5^+	$1s^12s^22p^1$	1.58	12		
	$1s^12s^12p^2$	6.56	60		
	$1s^12p^3$	9.64	40	7.13	2.38
6^+	$1s^12s^2$	0.29	2		
	$1s^12s^12p^1$	16.9	24		
	$1s^12p^2$	22.4	30	19.2	
7^+	$1s^12s^1$	75.0(0) [b]	4	55.4(75.0) [b]	
	$1s^12p^1$	48.9(1) [b]	12		

[a] Based upon the empirical formula of Larkins.
[b] The numbers in parentheses are obtained by neglecting the $2s$-$2p$ mixing.

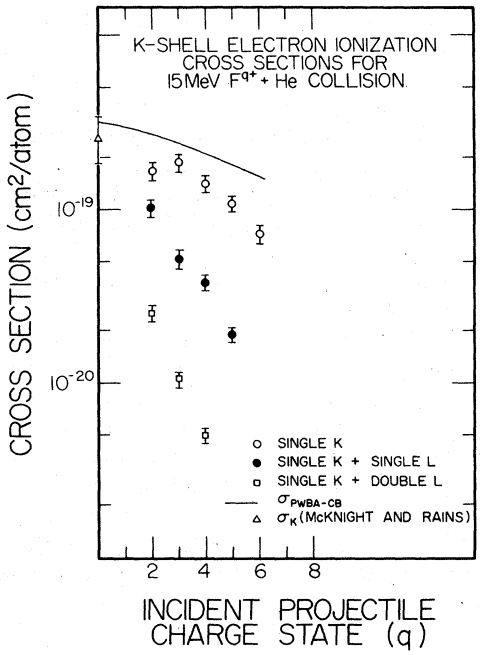

FIG. 12. F K-shell electron ionization cross sections for 15-MeV F^{q+}+He collisions. The open circles are for single K-shell electron ionization and the closed circles are for double ionization (single K-shell + single L-shell ionization). The open squares are for triple ionization (single K-shell + double L-shell ionization). The triangle denotes the measured cross section for neutral F atoms by McKnight and Rains (Ref. 22). The solid line is the calculated single K-shell ionization cross section based on the PWBA-CB.

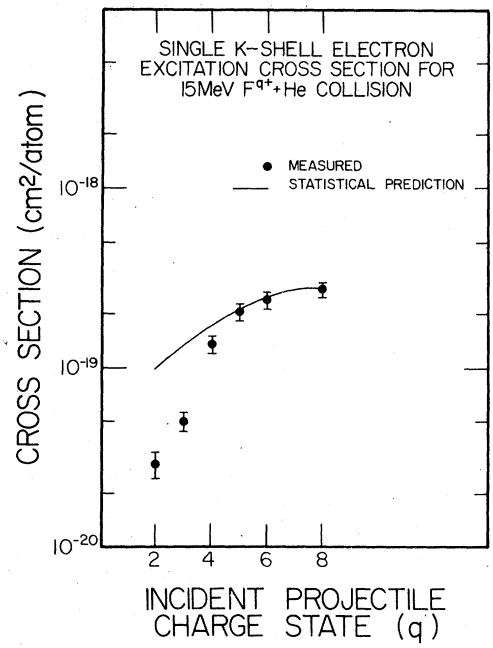

FIG. 13. F single K-shell electron excitation cross sections in 15-MeV F^{q+}+He collisions. The solid line represents the calculated cross section by assuming that the excitation cross sections are proportional to the number of L-shell vacancies (see text).

The calculated single K-shell electron ionization cross sections, based on the plane-wave Born approximation with Coulomb deflection and increased binding (PWBA-CB)[20] corrections, using the calculated binding energy for various ionization states are also given in Fig. 12. The calculated ionization cross sections do not decrease as rapidly as the measured cross sections. This could indicate that electron screening is effective for few electron ion systems on a light target like He.[21]

The cross section obtained by extrapolation to the neutral F atoms is in agreement with the results of McKnight and Rains[22] for bombardment of SF_6 with He ions and is also in agreement with the PWBA-CB prediction for neutral F atoms.

H. K-shell excitation cross sections for various charge states

The measured K-shell electron excitation cross sections (σ_{ee}) of F^{q+} are shown in Fig. 13. σ_{ee} increases one order of magnitude with increases in the charge states from F^{2+} to F^{6+}, and tends to saturate. For F^{7+} ions, σ_{ee} cannot be obtained accurately because of the unknown contribution of the metastable ^3S state in the beam. An estimate of this cross section is $\sim 2.8 \times 10^{-19}$ cm^2 assuming 15% of the beam in the ^3S state. The electron excitation cross sections per atom σ_{ee} shown in Fig. 13 for F^{9+} ions which have only one K-shell electron are multiplied by a factor of 2 in order to compare with the lower-charge-state ions which have two K-shell electrons. No theoretical calculations of σ_{ee} for various projectile charge states have been reported so far. The statistical prediction given in Fig. 13 is obtained by assuming the cross sections are proportional to the number of L vacancies and the number of K electrons. This prediction is arbitrarily normalized to the measured σ_{ee} for F^{6+} ions. The statistical calculation predicts the correct trend but overestimates the cross sections for low charge states. Ratios of σ_{ee} to σ_i are given in Fig. 14. The single K-shell ionization cross section increases drastically in going from F^{2+} to F^{6+}, indicating that the K-shell electron excitation processes become more important in x-ray production for higher-charge-state ions, compared with the K-shell electron ionization processes.

IV. CONCLUSION

We have used high-resolution K x-ray spectra to identify K x-ray transitions that are associated

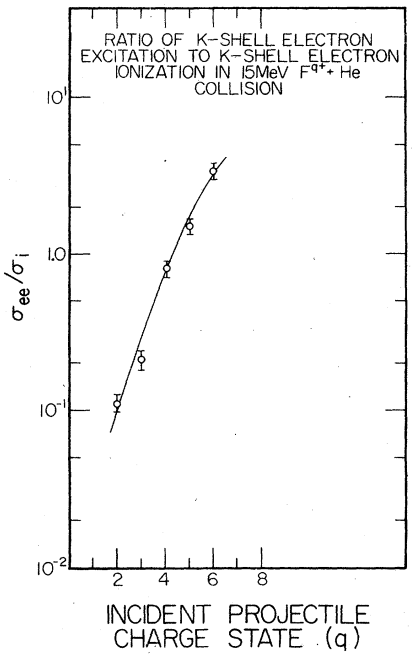

FIG. 14. Ratio of K-shell electron excitation to single K-shell electron ionization of 15-MeV F^{q+}+He collisions. The solid line is drawn to guide the eye.

with the three K x-ray production mechanisms of K-shell electron excitation, K-shell ionization, and electron capture to shells higher than the K shell. These production mechanisms have been studied as a function of the projectile charge state. We have obtained for the first time absolute cross sections for K-shell to L-shell excitation of F as a function of projectile charge state for F^{q+}+He collisions. We have also obtained the pure single K-shell ionization cross section as a function of projectile charge state for this system. For 15-MeV F^{q+} on He the ratio of the K-shell to L-shell excitation cross section to the single K-shell ionization cross section increases by more than one order of magnitude in going from $q = 2+$ to $q = 6+$. For $q = 4+$ the cross sections are nearly equal and for $q = 6+$ K-shell to L-shell excitation is about four times larger than single K-shell ionization. The charge dependence for the excitation cross section is qualitatively understood from a statistical calculation accounting for the number of initial L-shell holes and the number of initial K-shell electrons. The charge dependence for the single K-shell ionization cross section is in approximate agreement with a PWBA-CB calculation using the K-shell binding energies of F^{q+}. A study of the polarization of the projectile x rays[23] formed from the various processes leading to the various atomic configurations studied here would be of considerable interest. Theoretical calculations of the excitation, single and multiple ionization cross sections for projectiles with the various charge states are essential for understanding the collision phenomena involving the innershell electrons as well as the outershell electrons.

ACKNOWLEDGMENTS

The authors would like to thank Professor Chander Bhalla, Tom Tunnell, and Cuneyt Can for providing their calculations of the fluorescence yields and the transition energies prior to publication. This work was supported by the Division of Chemical Sciences, U. S. Department of Energy.

[1]P. Richard, in *Atomic Inner Shell Processes*, edited by B. Crasemann (Academic, New York, 1975), Vol. I, Chap. 2.
[2]R. L. Kauffman, K. A. Jamison, T. J. Gray, and P. Richard, Phys. Rev. Lett. 36, 1074 (1976).
[3]J. A. Demarest and R. L. Watson, Phys. Rev. A 17, 1302 (1978).
[4]F. Hopkins, R. L. Kauffman, C. W. Woods, and P. Richard, Phys. Rev. A 9, 2413 (1974).
[5]R. J. Fortner and D. L. Matthews, Phys. Rev. A 16, 1441 (1977).
[6]R. L. Blake (private communication).
[7]B. L. Henke and E. S. Ebisu, Adv. X-Ray Anal. 17, 150 (1974).
[8]P. Richard, R. L. Kauffman, F. F. Hopkins, C. W. Woods, and K. A. Jamison, Phys. Rev. Lett. 30, 888 (1973).
[9]E. P. Larkins, J. Phys. B 4, L29 (1971).
[10]R. L. Kauffman, C. W. Woods, F. F. Hopkins, D. O. Elliott, K. A. Jamison, and P. Richard, J. Phys. B 6, 2197 (1973).
[11]L. L. House, Astrophys. J. Suppl. 18, 21 (1969).
[12]T. Tunnell and C. P. Bhalla (private communication).
[13]J. Gesten, Phys. Rev. A 15, 940 (1977).
[14]J. R. Macdonald, P. Richard, C. L. Cocke, M. Brown, and I. A. Sellin, Phys. Rev. Lett. 31, 684 (1973).
[15]H. Tawara, P. Richard, K. A. Jamison, and T. J. Gray, J. Phys. B 11, L615 (1978).
[16]J. A. Guffey, Ph.D. thesis (Kansas State University, 1976) (unpublished).
[17]T. Tunnell and C. P. Bhalla (unpublished).
[18]C. P. Bhalla, Phys. Rev. A 12, 122 (1975).
[19]C. P. Bhalla, N. O. Folland, and M. A. Hein, Phys. Rev. A 8, 649 (1973).
[20]G. Basbas, W. Brandt, and R. Laubert, Phys. Rev. A 7, 983 (1973).
[21]F. K. Chen, G. Lapicki, R. Laubert, S. B. Elston, R. S. Peterson, and I. A. Sellin, Phys. Lett. A 60, 292 (1977).
[22]R. H. McKnight and R. G. Rains, Phys. Rev. A 14, 1388 (1976).
[23]L. D. Ellsworth, B. L. Doyle, U. Schiebel, and J. R. Macdonald (unpublished).